

Ultrathin Near-Infrared Light Activated Nano-Hotplate Catalyst

Xiangyang Wu and Edwin K. L. Yeow*

A combined photothermal-catalytic system that contains a single active element, without using different entities for separate roles (catalytic vs photothermal), is designed here for efficient catalytic reactions. Herein, ultrathin (sub-6 nm) rectangular-like KNdF₄ nanoplates consisting of 3–4 unit cell layers are prepared where the Nd³⁺ ions act as a Lewis acid catalyst. In addition, the nanoplates undergo light-to-heat conversion when irradiated with NIR light due to cross-relaxation and nonradiative relaxation processes from excited Nd³⁺. The cyanosilylation of a series of ketones is performed using the nano-hotplate catalysts to give near quantitative yields of the cyanohydrin trimethylsilyl ethers. This is because of the high surface area-to-volume ratio of the thin nanoplates that provides a large number of surface Nd³⁺ catalytic sites for reaction. The reaction kinetics are enhanced by the photothermal effect, leading to the observed > 10-fold increase in product yields.

Photothermal materials (PM) such as plasmonic nanocrystals (e.g., Au) and organic dyes (e.g., NIR dyes, porphyrins) are capable of converting light into heat. This property has enabled PM to drive reactions via a photothermal effect (e.g., in polymerization).^[1] When integrated with a separate catalyst, PM have also been shown to improve the efficiency of the catalyst used in a broad range of applications (e.g., in renewable energy, organic synthesis, and cancer therapy) by increasing the reaction temperature upon light irradiation.^[2] For example, metal–organic frameworks coupled with Pt nanocrystals were used for the photooxidation of alcohols,^[2a] and photothermal hybrid nanostructures were demonstrated to effectively catalyzed the conversion of CO₂ to fuels.^[2b] There are, however, existing issues that remain to be addressed including the poor photostability of photothermal dyes and morphology change of nanocrystals exposed to light (e.g., Au).^[3]

A promising group of PM is rare earth alkali tetrafluoride nanocrystals containing Nd³⁺ ions (e.g., NaNdF₄) and NdF₃ nanocrystals that undergo non-radiative relaxation, following near-infrared (NIR) light excitation and cross-relaxation within

pairs of closely spaced Nd³⁺,^[4,5] to yield light-to-heat conversion efficiencies (e.g., 0.21 for NaNdF₄ in chloroform) that are comparable to that of other nano-PMs (e.g., 0.24 for Au nanorods).^[6] In addition, Nd³⁺ is a good Lewis acid catalyst.^[7] For example, the addition of trimethylsilyl cyanide (TMSCN) to various aldehydes at ambient temperature has been carried out with Nd-containing materials as catalysts.^[8] However, the cyanosilylation of the less reactive ketones is often challenging; requiring longer reaction times and giving poorer product yields.^[8,9]

The goal of this study is the rational design of a neat two-in-one photothermal-catalyst that relies solely on only one active component to undergo photothermal conversion and act as a catalyst. To this end, we have prepared ultrathin (i.e., sub-6 nm

thickness) KNdF₄ nanoplates dispersed in polar solvents that release heat when excited by 808 nm light. At the same time, the Nd³⁺ ions in the nanoplates function as a Lewis acid catalyst. Employing thin nanoplates ensures that both the surface area-to-volume ratio and number of surface Nd³⁺ ions exposed to the reacting substrates are large. The combined photothermal-catalytic activity of the KNdF₄ nanoplate is demonstrated by performing cyanosilylation of a series of ketones in the presence of NIR light excitation. For all the ketones studied here, near quantitative product yields are observed within a short reaction time. Other advantages of our system are high photo- and thermal-stability, ease in recovering and recycling of the nanoplates, unchanged morphology after multiple use, activation by NIR photons hence avoiding direct excitation and photobleaching of organic substrates, and removing the use of cumbersome external heating appliances.

The KNdF₄ nanoplates were prepared using a coprecipitation method with a potassium/fluoride/rare-earth (K/F/Nd) ratio of 2.5:4:1.^[5] Further experimental details are provided in the Supporting Information. The growth mechanism of the as-prepared oleic acid (OA)/oleylamine (OAm)-capped KNdF₄ nanoplates was studied by examining the transmission electron microscopy (TEM) images and X-ray diffraction (XRD) patterns of nanocrystals obtained at various reaction times t_r . At the start of the reaction, when the temperature first reaches the reaction temperature $T_r = 306\text{ }^{\circ}\text{C}$ (i.e., $t_r = 0\text{ min}$), the TEM image shows small nanoparticles (average radius = $4.4 \pm 0.5\text{ nm}$) (Figure 1A and Figure S1, Supporting Information). When t_r is extended to 30 min, both small nanoparticles and large rectangular-like nanoplates are seen (Figures 1B). When t_r is further increased

Dr. X. Wu, Prof. E. K. L. Yeow
Division of Chemistry and Biological Chemistry
School of Physical and Mathematical Sciences
Nanyang Technological University
21 Nanyang Link, Singapore 637371, Singapore
E-mail: edwinyeow@ntu.edu.sg

The ORCID identification number(s) for the author(s) of this article can be found under <https://doi.org/10.1002/sml.202002698>.

DOI: 10.1002/sml.202002698

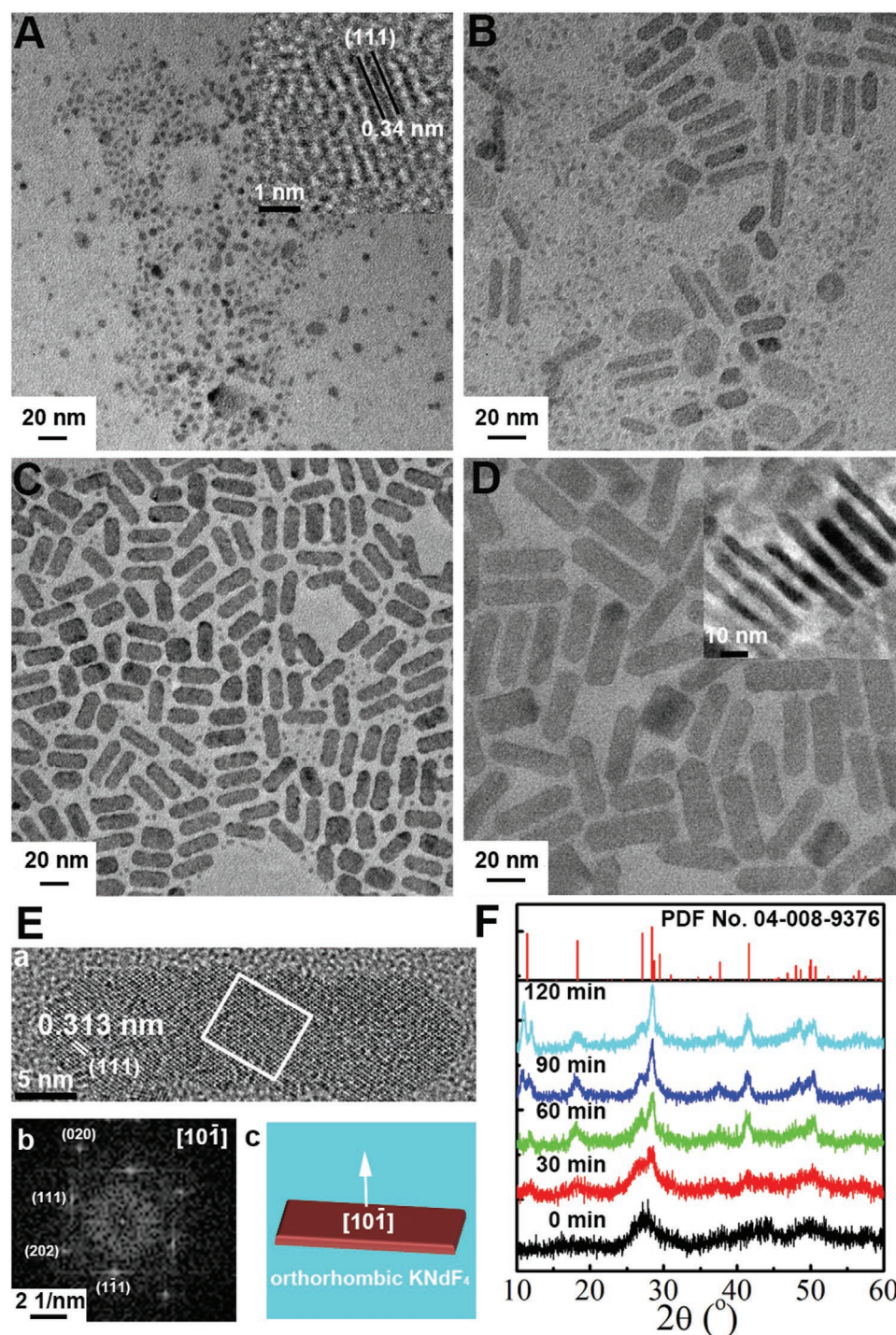


Figure 1. TEM images of the products obtained at 306 °C for different reaction times A) 0 min; B) 30 min; C) 60 min; D) 120 min. Inset of (A) is the HRTEM image of a single nanoparticle and inset of (D) is the TEM image of single nanoplates standing on their edge. E-a) HRTEM image of a single nanoplate with a length of 34.1 nm and width of 10.2 nm, b) the FFT pattern with $[10\bar{1}]$ zone axis for the white-boxed area in (a), and c) schematic of nanoplate. F) XRD patterns of the products obtained at 306 °C for different reaction times and the standard XRD pattern of orthorhombic KNdF_4 (PDF entry no.: 04-008-9376).

to 60 min, the major product obtained are nanoplates albeit in the presence of a small number of nanoparticles (Figure 1C). For $t_r = 90$ and 120 min, only rectangular-like nanoplates are formed (Figure 1D). Both the average length $\langle L \rangle$ and width $\langle W \rangle$

of the nanoplates increase with reaction time with $\langle L \rangle = 40.3 \pm 9.1$ nm and $\langle W \rangle = 16.7 \pm 0.9$ nm for $t_r = 120$ min (Figures S1 and S2 and Table S1, Supporting Information). The thickness of the latter, determined from the TEM image of the nanoplates

standing on their edge, is $\langle D \rangle = 4.3 \pm 0.6$ nm (inset of Figure 1D and Figure S2, Supporting Information).

The XRD pattern of the nanoparticles in Figure 1A displays peaks that are indexed to cubic KNdF₄ with bands centered at $2\theta = 27.9^\circ$ (comprising of peaks corresponding to the (111) and (200) lattice planes), 40.8° (corresponding to the (220) lattice plane) and 50.0° (corresponding to the (311) lattice plane) (Figure 1F).^[10] The broad bands indicate poorly crystallized material. The assignment to cubic phase is further supported by the (111) lattice plane with lattice distance = 0.34 nm in the high-resolution TEM (HRTEM) image (inset of Figure 1A).^[10]

The XRD patterns obtained for $t_r \geq 30$ min display diffraction peaks that matched those of standard orthorhombic KNdF₄ (PDF No. 04-008-9376) with the bands, centered at $2\theta = 11.0^\circ$ (corresponding to the (002) lattice plane), 28.5° (corresponding to the (111) lattice plane), 41.6° (corresponding to the (213) lattice plane), and 50.7° (corresponding to the (311) lattice plane), becoming sharper with t_r (Figure 1F). The rectangular-like nanoplates whose crystallinity improves with reaction time are ascribed to orthorhombic phase KNdF₄. The HRTEM image of a nanoplate lying flat on its face reveals an interplanar spacing of 0.313 nm (Figure 1E-a), corresponding to the (111) lattice plane of orthorhombic KNdF₄. Furthermore, the fast Fourier transform (FFT) pattern in Figure 1E-b are assigned to the lattice planes of orthorhombic KNdF₄ (i.e., (111), (202), (020), and $(1\bar{1}1)$) with a $[10\bar{1}]$ zone axis. Therefore, layers of KNdF₄ are stacked along the $[10\bar{1}]$ direction (Figure 1E-c), and the nanoplate grows preferentially along the two directions perpendicular to each other and to the zone axis. The coordination number (CN) of Nd in cubic KNdF₄ is 8 whereas it is 9 in the orthorhombic structure.^[11] In general, a higher CN confers greater stability to the compound. As the reaction progresses, the growth of KNdF₄ nanoplates follows Ostwald ripening with unstable cubic KNdF₄ nanoparticles undergoing dissolution into monomers which are redeposited onto the more stable orthorhombic nanoplates.

The OA/OAm-capped KNdF₄ nanoplates were successfully transferred to dimethylformamide (DMF) to form a clear dispersion following treatment with the exchange ligand nitrosonium tetrafluoroborate (NOBF₄).^[12] The attenuated total reflection-Fourier transform infrared (ATR-FTIR) spectrum of the nanoplates in DMF overlaps with that of pure DMF solution (Figure S3, Supporting Information). Furthermore, typical bands arising from asymmetric ($\nu_{as}(\text{CO}_2^-)$, 1545 cm^{-1}), and symmetric ($\nu_s(\text{CO}_2^-)$, 1454 cm^{-1}) stretching vibrations of the carboxylic group of surfaces oleate are not detected when compared to OA/OAm-capped KNdF₄ nanoplates (Figure S3, Supporting Information). This indicates that the OA/OAm ligands are effectively removed by NOBF₄. The morphology of the nanoplates remain invariant after ligand exchange (Figure S4, Supporting Information).

Figures 2A,B shows the time-resolved photothermal response profiles and thermal images of a DMF solution containing KNdF₄ nanoplates during NIR laser excitation (808 nm, 1.15 W cm^{-2}) in ambient conditions. The temperature of the sample increases with time and the maximum change in temperature $\Delta T \approx 15.2^\circ\text{C}$ is attained within 360 s of light irradiation. The photothermal heat is likely generated from nonradiative relaxation from the $^4I_{15/2}$ state to $^4I_{9/2}$ state of Nd³⁺

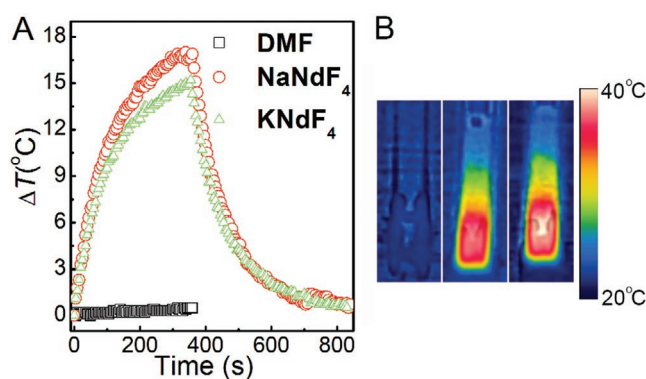


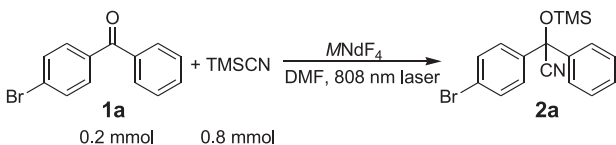
Figure 2. A) Temperature change profiles of DMF solutions in the absence and presence of NaNdF₄ nanorods and KNdF₄ nanoplates excited using an 808 nm laser and B) the corresponding thermal images taken after 360 s of light irradiation (from left to right: DMF, DMF with KNdF₄ nanoplates, and DMF with NaNdF₄ nanorods).

ions after cross-relaxation (Figure S5, Supporting Information). When the laser source is turned off, the temperature gradually returns to room temperature (21.5°C) within 480 s. The light-to-heat conversion efficiency of KNdF₄ nanoplates in DMF is $\eta = 25.6\%$ (Figures S6 and S7, Supporting Information). The nanoplates also display good photothermal stability where after five continuous heating/cooling cycles, the ΔT value remains unchanged (i.e., $\Delta T \approx 15.3^\circ\text{C}$ in the fifth cycle, Figure S8, Supporting Information).

The enhanced efficiency of the cyanosilylation of ketones with TMSCN using KNdF₄ nanoplates as a two-in-one hotplate catalyst is demonstrated here. We begin by performing controlled experiments for the reaction between 4-bromobenzophenone **1a** and TMSCN in DMF solvent. At room temperature and in the absence of both KNdF₄ nanoplates and 808 nm light irradiation, trace amounts of product **2a** is formed after 4 min reaction time; DMF is therefore unable to catalyze the reaction (entry 1 in Table 1). When the reaction mixture is exposed to 808 nm light (intensity $I = 4.3\text{ W cm}^{-2}$) for 4 min, a small increase in temperature ($<5^\circ\text{C}$) and low product yield are observed (entry 2 in Table 1). The effects of elevated temperature is also studied by raising the temperature of the mixture to 55°C within 70 s and then maintaining the temperature between 55 and 57°C for a further 170 s via a preheated water bath (i.e., reaction time of 4 min, see temperature profile in Figure S9 in the Supporting Information) (condition a). In this case, the product yield is improved to 34% (entry 3 in Table 1) but remains relatively low.

When KNdF₄ nanoplates (4.8 mol%) are added into a mixture containing **1a** and TMSCN, a product yield of 30% is observed after 4 min reaction time at room temperature (entry 4 in Table 1) (condition b). Reducing the KNdF₄ nanoplate loading (e.g., 2.5 mol%) leads to a decrease in product yield (entry 5 in Table 1) and vice versa (e.g., 9.2 mol%, entry 6 in Table 1). Therefore, the yield of **2a** is dependent on the amount of nanoplates employed and increases with catalyst load and Nd³⁺ catalytic sites. To study the effects of light irradiation, a mixture containing **1a**, TMSCN and 4.8 mol% KNdF₄ nanoplates was irradiated with 808 nm light ($I = 4.3\text{ W cm}^{-2}$) for 4 min (condition c). As a result of photothermal conversion, the temperature of the reaction mixture increases to 52°C within

Table 1. Cyanosilylation of 4-bromobenzophenone **1a** with TMSCN under various conditions. The reaction time for each condition is 4 min.



| Entry | KNdF ₄ [x mol%] | Light intensity [W cm ⁻²] ^{a)} | Yield [%] ^{b)} |
|------------------|---------------------------------------|---|-------------------------|
| 1 ^{c)} | — | — | 1 |
| 2 | — | 4.3 | 6 |
| 3 ^{d)} | — | — | 34 |
| 4 ^{e)} | KNdF ₄ (4.8) | — | 30 |
| 5 ^{e)} | KNdF ₄ (2.5) | — | 16 |
| 6 ^{e)} | KNdF ₄ (9.2) | — | 59 |
| 7 ^{f)} | KNdF ₄ (4.8) | 4.3 | 99 |
| 8 ^{f)} | KNdF ₄ (4.8) | 1.4 | 82 |
| 9 ^{e)} | NaN ₂ F ₄ (5.1) | — | 17 |
| 10 ^{f)} | NaN ₂ F ₄ (5.1) | 4.3 | 73 |

^{a)}808 nm laser light; ^{b)}NMR yield; ^{c)}Room temperature; ^{d)}Condition a: no catalyst and no NIR light irradiation but with elevated temperature; ^{e)}Condition b: with catalyst at room temperature and no NIR light irradiation; ^{f)}Condition c: with catalyst and NIR light irradiation.

70 s and maintained between 52 and 55 °C for a further 170 s according to the temperature profile given in Figure S9 (Supporting Information). In this case, quantitative product yield is observed (entry 7 in Table 1). Reducing the light intensity to $I = 1.4 \text{ W cm}^{-2}$ leads to a solution temperature of $\approx 34 \text{ °C}$ and decreased product yield (82%, entry 8 in Table 1) (Figure S10, Supporting Information). The catalytic activity of the KNdF₄ nanoplates is thus significantly enhanced when exposed to NIR light and is dependent on light intensity.

The KNdF₄ nanoplates can also be recycled for use without compromising their morphology nor catalytic activity. Five successive runs involving **1a** using the same batch of recovered KNdF₄ nanoplates under condition c provided near quantitative product yields for all the runs (Figure S11, Supporting Information). In addition, the morphology of the nanoplates remains intact throughout as demonstrated by the TEM image of the nanoplates recorded after the fifth run (Figure S12, Supporting Information).

The cyanosilylation of **1a** in the presence of hexagonal phase NaN₂F₄ nanorods (CN of Nd is 9)^[13] of average length $44.2 \pm 3.7 \text{ nm}$ and average width $26.5 \pm 1.8 \text{ nm}$ (Figure S13, Supporting Information) was performed to assess the benefits of thin nanoplates against thicker nanorods.^[5] The photothermal efficiency of NaN₂F₄ nanorods in DMF is $\eta = 32.4\%$ (Figures S6 and S7, Supporting Information). Without light irradiation, the yield of **2a** is 17% when NaN₂F₄ nanorods (5.1 mol%; similar mass as nanoplates used in entries 4 and 7, Table 1) are used as catalyst for reaction at room temperature (entry 9, Table 1), and increases to 73% upon 808 nm light excitation for 4 min (i.e., solution temperature due to photothermal conversion is 63 °C, Figure S9, Supporting Information) (entry 10, Table 1). In this case, the rate of product formation is lower than that when KNdF₄ nanoplates are used (entry 7, Table 1). To rationalize this difference, the ratio of the surface area per gram of KNdF₄

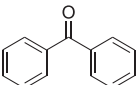
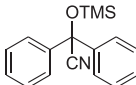
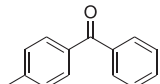
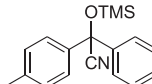
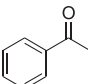
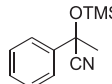
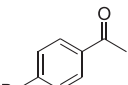
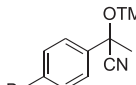
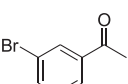
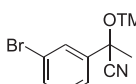
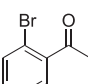
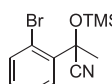
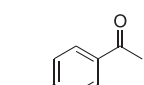
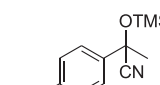
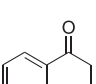
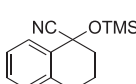
nano-plates and NaN₂F₄ nanorods is calculated to be 3.45 (Supporting Information). Furthermore, a nanoplate comprises of $\approx 3\text{--}4$ layers of KNdF₄ unit cells of which half of the total Nd³⁺ ions are found at the outermost layer or surface (i.e., 45%, Supporting Information). This is in contrast with only 18% of surface Nd³⁺ for the case of NaN₂F₄ nanorods (Supporting Information). For example, the amount of surface Nd³⁺ ions is $\approx 1.74 \text{ mmol g}^{-1}$ for KNdF₄ nanoplates as compared to only 0.74 mmol g^{-1} for NaN₂F₄ nanorods. Clearly, the larger total surface area of thin KNdF₄ nanoplates provides an increased number of exposed Nd³⁺ ions and potentially more active defect sites (e.g., coordinatively unsaturated Nd) for reaction.^[8a,b] However, the exact nature of the latter is still unknown.

The cyanosilylations of other ketones (**1b–1i**, Table 2) with TMSCN are also investigated and the results presented in Table 2. For the control experiment using NIR irradiation only in the absence of catalyst, the product yields obtained for **1b–1i** are negligible (Table S2, Supporting Information). When either condition a (i.e., elevated temperature of 55–57 °C by external water bath and in the absence of nanoplates and NIR light irradiation) or condition b (i.e., reaction in the presence of 4.8 mol% KNdF₄ nanoplates for 4 min without light irradiation) is employed, the yields of cyanohydrin trimethylsilyl ethers **2b–2i** are low (Table 2). This is in agreement with the work of Wang et al. who reported low efficiency for the cyanosilylation of ketones in a catalyst-free environment under elevated reaction temperature.^[14] On the other hand, exposing the reaction mixture containing the nanoplates to 808 nm light ($I = 4.3 \text{ W cm}^{-2}$) for 4 min (condition c) produces exceptionally good product yields of **2b–2i** with the majority of ketones achieving >90% yields.

A three-step mechanism, illustrated in Figure 3, as a possible mechanism for the cyanosilylation reaction by Nd³⁺-based Lewis acid catalysts (e.g., NdF₃ particles and Nd³⁺-based metal-organic framework (MOFs)) has previously been discussed by others.^[8a,b,15] Briefly, it involves a coordination of the O in the ketone to Nd³⁺ in the nanoplate (step 1), attack of the CN group in TMSCN to the carbonyl group in the ketone (step 2), and isomerization of the Si(CH₃)₃ group to form the product (step 3). To evaluate the role of localized heating effect on the surface of the KNdF₄ nanoplates,^[1a] the cyanosilylation of ketones **1a–1i** were repeated in the presence of the nanoplates (4.8 mol%) at an elevated temperature ($\approx 55 \text{ °C}$) achieved by water bath heating (i.e., no NIR irradiation) (Figure S9, Supporting Information). After a reaction time of 4 min, good product yields, similar to the ones obtained with photothermal heating (Tables 1 and 2), were noted (Table S3, Supporting Information). This indicates that an increased temperature of the surrounding solvent, rather than localized surface heating, is sufficient to improve the efficiency of the reaction. Photothermal heating therefore leads to more collisions between ketones and nanoplates, and between substrates. The rate constant for reaction is also improved with a higher reaction temperature.

In summary, we have demonstrated the design and application of KNdF₄ nanoplates as a two-in-one photothermal-catalyst that uses only one active component (Nd³⁺) as both the Lewis acid catalytic site and light-to-heat converting element. We show the exceptionally good product yields when the nano-hotplates are used for the cyanosilylation of relatively inert ketones.

Table 2. Cyanosilylation of ketones **1b–1i** with TMS-CN under condition a, b, or c. The reaction time for each condition is 4 min.

| | | $\text{R}_1-\text{C}(=\text{O})-\text{R}_2 + \text{TMS-CN} \xrightarrow{\text{Condition a, b, or c}} \text{R}_1-\text{C}(\text{OTMS})(\text{CN})-\text{R}_2$ | | | | |
|---|-----------|--|-----------|-------------------------|-------------------------|-------------------------|
| Ketones | | Products | | Yield [%] ^{a)} | Yield [%] ^{b)} | Yield [%] ^{c)} |
|  | 1b |  | 2b | 3 | 3 | 99 |
|  | 1c |  | 2c | 2 | 6 | 99 |
|  | 1d |  | 2d | 0 | 0 | 92 |
|  | 1e |  | 2e | 0 | 16 | 94 |
|  | 1f |  | 2f | 7 | 26 | 97 |
|  | 1g |  | 2g | 0 | 7 | 99 |
|  | 1h |  | 2h | 1 | 4 | 95 |
|  | 1i |  | 2i | 2 | 3 | 96 |

^{a)}Condition a: no catalyst and no NIR light irradiation but with elevated temperature; ^{b)}Condition b: with catalyst at room temperature and no NIR light irradiation; ^{c)}Condition c: with catalyst and NIR light irradiation.

The thin nanoplates are advantageous due to a higher total number of surfaces Nd^{3+} ions and defect sites exposed to the reacting substrates, whereas the increased temperature from

photothermal effects enhances the reaction kinetics. Our study opens up a new avenue for the utilization of simple lanthanide-based nanomaterials as multifunctional catalysts.

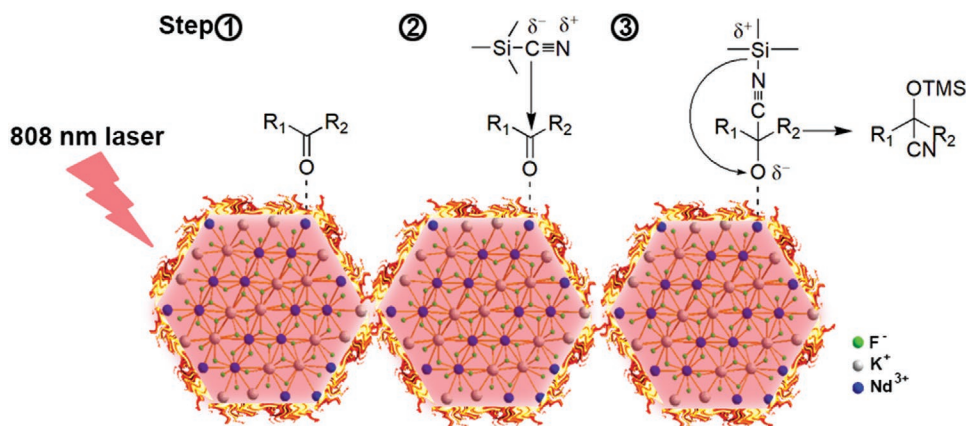


Figure 3. Scheme of cyanosilylation reaction catalyzed by KNdF_4 nanoplates upon NIR-light excitation.

Supporting Information

Supporting Information is available from the Wiley Online Library or from the author.

Acknowledgements

E.K.L.Y. acknowledges the Singapore Ministry of Education MoE Tier 1 fund (RG6/18) for financial support.

Conflict of Interest

The authors declare no conflict of interest.

Keywords

cyanosilylation, lanthanide-based nanomaterials, Lewis acid catalysts, photothermal effects, two-in-one catalysts

Received: April 29, 2020

Revised: July 2, 2020

Published online:

- [1] a) K. M. Haas, B. J. Lear, *Chem. Sci.* **2015**, *6*, 6462; b) R. C. Steinhardt, T. M. Steeves, B. M. Wallace, B. Moser, D. A. Fishman, A. P. Esser-Kahn, *ACS Appl. Mater. Interfaces* **2017**, *9*, 39034; c) A.-H. Bonardi, F. Bonardi, F. Morlet-Savary, C. Dietlin, G. Noirbent, T. M. Grant, J.-P. Fouassier, F. Dumur, B. H. Lessard, D. Gimes, J. Lalevée, *Macromolecules* **2018**, *51*, 8808; d) Q. Yang, Q. Xu, S.-H. Yu, H.-L. Jiang, *Angew. Chem., Int. Ed.* **2016**, *55*, 3685; e) B. Jin, Y. Li, J. Wang, F. Meng, S. Cao, B. He, S. Jia, Y. Wang, Z. Li, X. Liu, *Small* **2019**, *15*, 1903847.
- [2] a) Y.-Z. Chen, Z. U. Wang, H. Wang, J. Lu, S.-H. Yu, H.-L. Jiang, *J. Am. Chem. Soc.* **2017**, *139*, 2035; b) M. Ghousoub, M. Xia, P. N. Duchesne, D. Segal, G. Ozin, *Energy Environ. Sci.* **2019**, *12*, 1122; c) H. Huang, L. Zhang, Z. Lv, R. Long, C. Zhang, Y. Lin, K. Wei, C. Wang, L. Chen, Z.-Y. Li, Q. Zhang, Y. Luo, Y. Xiong, *J. Am. Chem. Soc.* **2016**, *138*, 6822; d) G. M. Neelgund, A. Oki, *Mater. Chem. Front.* **2018**, *2*, 64; e) H.-C. Ma, C.-C. Zhao, G.-J. Chen, Y.-B. Dong, *Nat. Commun.* **2019**, *10*, 3368; f) Q. Zhang, Q. Guo, Q. Chen, X. Zhao, S. J. Pennycook, H. Chen, *Adv. Sci.* **2020**, *7*, 1902576.
- [3] a) G. Chen, J. Damasco, H. Qiu, W. Shao, T. Y. Ohulchanskyy, R. R. Valiev, X. Wu, G. Han, Y. Wang, C. Yang, H. Ågren, P. N. Prasad, *Nano Lett.* **2015**, *15*, 7400; b) S. Link, C. Burda, B. Nikoobakht, M. A. El-Sayed, *J. Phys. Chem. B* **2000**, *104*, 6152.
- [4] a) A. Bednarkiewicz, D. Wawrzynczyk, M. Nyk, W. Strek, *Appl. Phys. B* **2011**, *103*, 847; b) D. Wawrzynczyk, A. Bednarkiewicz, M. Nyk, W. Strek, M. Samoc, *Nanoscale* **2012**, *4*, 847.
- [5] X. Wu, E. K. L. Yeow, *Nanoscale* **2019**, *11*, 15259.
- [6] a) Q. Tian, F. Jiang, R. Zou, Q. Liu, Z. Chen, M. Zhu, S. Yang, J. Wang, J. Wang, J. Hu, *ACS Nano* **2011**, *5*, 9761; b) C. M. Hessel, V. P. Pattani, M. Rasch, M. G. Panthani, B. Koo, J. W. Tunnell, B. A. Korgel, *Nano Lett.* **2011**, *11*, 2560.
- [7] M. Shibasaki, K. Yamada, N. Yoshikawa in *Lewis Acids in Organic Synthesis* (Ed: H. Yamamoto), Wiley-VCH, Weinheim **2000**.
- [8] a) X. Kang, W. Shang, Q. Zhu, J. Zhang, T. Jiang, B. Han, Z. Wu, Z. Li, X. Xing, *Chem. Sci.* **2015**, *6*, 1668; b) R. F. D'Vries, M. Iglesias, N. Snejko, E. Gutiérrez-Puebla, M. A. Monge, *Inorg. Chem.* **2012**, *51*, 11349; c) K. Suzuki, M. Sugawa, Y. Kikukawa, K. Kamata, K. Yamaguchi, N. Mizuno, *Inorg. Chem.* **2012**, *51*, 6953; d) F. Wang, Y. Wei, S. Wang, X. Zhu, S. Zhou, G. Yang, X. Gu, G. Zhang, X. Mu, *Organometallics* **2015**, *34*, 86; e) L. Mei, M. H. Zhu, *Synth. Commun.* **2005**, *35*, 2615.
- [9] a) G. K. S. Prakash, H. Vaghoo, C. Panja, V. Surampudi, R. Kultyshev, T. Mathew, G. A. Olah, *Proc. Natl. Acad. Sci. USA* **2007**, *104*, 3026; b) A. Procopio, G. Das, M. Nardi, M. Oliverio, L. Pasqua, *ChemSusChem* **2008**, *1*, 916; c) W. Wang, M. Luo, J. Li, S. A. Pullarkat, M. Ma, *Chem. Commun.* **2018**, *54*, 3042; d) M. Bandini, P. G. Cozzi, A. Garelli, P. Melchiorre, A. Umani-Ronchi, *Eur. J. Org. Chem.* **2002**, 3243; e) J.-M. Brunel, I. P. Holmes, *Angew. Chem., Int. Ed.* **2004**, *43*, 2752.
- [10] Y.-P. Du, Y.-W. Zhang, L.-D. Sun, C.-H. Yan, *Dalton Trans.* **2009**, 8574.
- [11] N. I. Sorokin, *Crystallogr. Rep.* **2016**, *61*, 55.
- [12] A. Dong, X. Ye, J. Chen, Y. Kang, T. Gordon, J. M. Kikkawa, C. B. Murray, *J. Am. Chem. Soc.* **2011**, *133*, 998.
- [13] Q. Dou, Y. Zhang, *Langmuir* **2011**, *27*, 13236.
- [14] W. Wang, M. Luo, W. Yao, M. Ma, S. A. Pullarkat, L. Xu, P.-H. Leung, *ACS Sustainable Chem. Eng.* **2019**, *7*, 1718.
- [15] Z. Hu, D. Zhao, *CrystEngComm* **2017**, *19*, 4066.